Kelvin wave in miscible two-component Bose-Einstein condensates

Kenichi Kasamatsu,[1] Maki Okada,[1] and Hiromitsu Takeuchi[2]
[1]*Department of Physics, Kindai University, Higashi-Osaka, Osaka 577-8502, Japan*
[2]*Department of Physics and Nambu Yoichiro Institute of Theoretical and Experimental Physics, Osaka Metropolitan University, Osaka 558-8585, Japan*

(Received 29 September 2022; accepted 9 January 2023; published 18 January 2023)

We study the dispersion relation of Kelvin waves propagating along single- and half-quantum vortices in miscible two-component Bose-Einstein condensates based on the analysis of the Bogoliubov–de Gennes equation. With the help of the interpolating formula connecting the dispersion relations in low- and high-wave-number regimes, we reveal the nontrivial dependence of the dispersion relation on the intercomponent interaction through the change in the vortex-core size of the vortical component. We also find the splitting of the Kelvin wave dispersion into gapless and gapped branches when both components have overlapping single-quantized vortices.

DOI: 10.1103/PhysRevA.107.013309

I. INTRODUCTION

Quantized vortices play a leading role in macroscopic quantum phenomena associated with superfluidity, thoroughly studied in, e.g., liquid helium [1], cold atomic gases [2], and exciton-polariton condensates [3]. Vortices in three-dimensional superfluids form lines that may be linear or curved and can possess axial wave excitations propagating along vortex lines. The gapless excitation involving helical deformation of a vortex line is known as the "Kelvin wave" [4,5]. Kelvin waves can exist in low-temperature superfluids and have been discussed intensively in the context of the decay mechanism of quantum turbulence [6–13].

A study of vortex waves in cold atomic Bose-Einstein condensates (BECs) has some advantages compared with that in other superfluid systems. Experimentally, a vortex can be created in a well-controlled manner, e.g., by means of an external rotation [14], phase engineering [15], and a moving obstacle [16]. Excitations of vortex waves are closely related to collective modes of the BEC [17]. Also, vortex dynamics can be visualized by optical techniques, which enable us to make direct measurements of the three-dimensional dynamics of vortex lines [18,19]. Theoretically, the vortex states can be well described by the Gross-Pitaevskii (GP) mean-field theory [20]. The excitation spectrum of the Kelvin wave and other vortex waves can be studied by the linearization analysis based on the Bogoliubov-de Genne (BdG) equation and direct numerical simulations of the GP equations [21–26].

In this work, we discuss a nontrivial case, namely, Kelvin waves in miscible two-component BECs. Two-component (binary) BECs with tunable interatomic interactions have been realized in cold atomic gases [27–30]. The salient feature in this system is caused by the presence of interatomic interactions between the different components, which determine, for example, the miscibility or immiscibility of the ground-state structure. Although vortex dynamics in a binary superfluid system have been studied in various situations, most of them are restricted in the two-dimensional analysis [31–44]. Although Hayashi *et al.* considered, through a three-dimensional analysis, the dynamical instability of helical shear flows of binary BECs [45], in which one flows along the core of the vortex line of the other component, their analysis was restricted to the immiscible case.

A vortex in miscible two-component BECs takes a rich variety of core structures [46]. When the first component has a vortex, the nonvortex second component is influenced by the presence of the vortex core; the density of the second component fills in the vortex core so that the superfluid order parameter does not vanish there. As the second component feels the density distribution of the first component as the potential well, the second component forms a density peak (minimum) at the vortex axis for repulsive (attractive) intercomponent interaction. When there are vortices in both components, such an attractive intercomponent interaction causes overlapping of the vortex cores [47]. This variety of vortex structures makes us expect the nontrivial dispersion relation of the vortex waves, compared with that of the single-component one. We calculate the dispersion relation of the Kelvin wave through the BdG analysis to study the impact arising from intercomponent interaction on the properties of the Kelvin wave. We find that the Kelvin wave dispersion is well described by the formula that interpolates the quadratic + logarithmic form in a low-wave-number regime and the quadratic form in a high-wave-number regime, depending on the intercomponent interaction only through the vortex thickness.

This paper is organized as follows. In Sec. II, we briefly review the properties of the Kelvin wave in a single-component BEC and introduce the interpolating method. Next, we turn to the problem of the two-component BECs, discussing the dynamical stability of the vortex states in Sec. III A and giving a detailed evaluation of the vortex-core size in Sec. III B. The analyses of the BdG equations for the Kelvin wave are described in Sec. IV. We conclude the paper in Sec. V.

II. KELVIN WAVE IN A SINGLE-COMPONENT BOSE-EINSTEIN CONDENSATE

First, we briefly review the Kelvin wave excitations in a single-component BEC based on the microscopic analysis of the BdG equation. We consider a straight vortex line in a dilute gaseous BEC confined in a cylinder. The vortex state can be obtained by solving the stationary GP equation $(\hat{h} + g|\Psi|^2)\Psi = \mu\Psi$, where $\hat{h} = -\hbar^2\nabla^2/(2M) + V_{\rm ext}(\boldsymbol{r})$ is the single-particle Hamiltonian with atomic mass M and external potential $V_{\rm ext}(\boldsymbol{r})$. The parameter g is the coupling constant, given by the s-wave scattering between cold atoms. The chemical potential μ determines the equilibrium bulk density $n = \mu/g$ far from the boundary. In the following, we consider the homogeneous system [$V_{\rm ext}(\boldsymbol{r}) = 0$] in the cylindrical coordinates $\boldsymbol{r} = (r, \theta, z)$.

The stationary vortex solution can be written in the axisymmetric form $\Psi(\boldsymbol{r}) = f(r)e^{iq\theta}$ with the real function $f(r)$ and the vortex winding number q; the solution has translation symmetry along the z axis. We impose the Neumann boundary condition at $r = R$ as $f'(R) = 0$, where the prime means the derivative by r. Also, we impose $f(0) = 0$ and $f'(0) = 0$ for $q \neq 0$ and $q = 0$, respectively. The radial profile of the vortex state with $q = 1$, depicted in Fig. 1(a), shows that the density becomes zero at the vortex core and heals from zero to the bulk value n in the scale of the healing length $\xi = \hbar/\sqrt{Mgn}$. We do not consider a vortex with $q \geqslant 2$, which is dynamically unstable [48–53].

Next, we consider the fluctuation around the stationary vortex solution. The wave function is taken to be $\Psi(\boldsymbol{r}, t) = \Psi(\boldsymbol{r}) + \delta\Psi(\boldsymbol{r}, t)$, where the fluctuation can be written as

$$\delta\Psi(\boldsymbol{r}, t) = e^{iq\theta - i\mu t/\hbar}[u(\boldsymbol{r}, t) - v^*(\boldsymbol{r}, t)], \tag{1}$$

and the amplitudes $u(\boldsymbol{r}, t)$ and $v(\boldsymbol{r}, t)$ are set as

$$u(\boldsymbol{r}, t) = \sum_{m,l,k_z} u_{mlk_z}(r)e^{i(l\theta + k_z z - \omega t)}, \tag{2}$$

$$v(\boldsymbol{r}, t) = \sum_{m,l,k_z} v_{mlk_z}(r)e^{i(l\theta + k_z z - \omega t)}. \tag{3}$$

Here, m and l represent the quantum numbers of the radial mode and the azimuthal mode, respectively, and k_z is the axial wave number along the z axis. The radial profiles $u_{mlk_z}(r)$ and $v_{mlk_z}(r)$, which are real functions, depend on these quantum numbers and are obtained by solving the coupled BdG equation

$$\mathcal{H}^{(lk_z)}\boldsymbol{w}_{mlk_z} = \hbar\omega\boldsymbol{w}_{mlk_z}. \tag{4}$$

This equation yields the eigenvalue $\omega = \omega_{mlk_z}$ and the eigenvector $\boldsymbol{w}_{mlk_z} = [u_{mlk_z}(r), v_{mlk_z}(r)]^{\rm T}$. The matrix $\mathcal{H}^{(lk_z)}$ is given by

$$\mathcal{H}^{(lk_z)} = \begin{pmatrix} \hat{h}^+_{lk_z} & -gf(r)^2 \\ gf(r)^2 & -\hat{h}^-_{lk_z} \end{pmatrix}, \tag{5}$$

with

$$\hat{h}^\pm_{lk_z} = \frac{\hbar^2}{2M}\left(-\frac{\partial^2}{\partial r^2} - \frac{1}{r}\frac{\partial}{\partial r} + \frac{(q \pm l)^2}{r^2} + k_z^2\right) - \mu + 2gf^2. \tag{6}$$

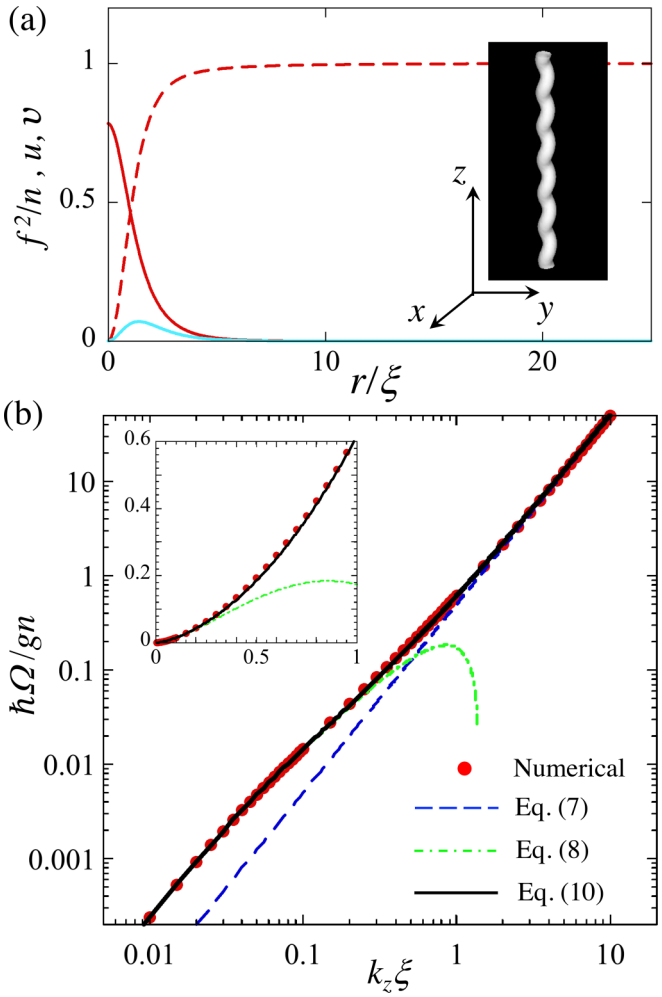

FIG. 1. In (a), we plot the profile of the stationary solution with a vortex at $r = 0$ (red dashed curve) and the Bogoliubov amplitudes $u_{mlkz}(r)$ (dark red curve) and $v_{mlkz}(r)$ (light blue curve) with $(m, l, k_z) = (0, -1, \xi^{-1})$ for a single-component BEC in a cylinder; u and v are not normalized. The insets show the isosurface of $|\Psi + \delta\Psi|^2 = 0.8n$ for the Kelvin mode with $k_z\xi = 1$ within the region $|z| \leqslant 20\xi$. (b) shows the dispersion relation of the Kelvin wave with $l = -1$ with $R = 30\xi$ [54]. The result shown by the red dots is obtained by solving the BdG equation (4) numerically. We show the log-log plot of the data, where the small negative shift $\Delta/\mu \simeq -10^{-3}$ at $k_z = 0$ is subtracted. The blue dashed line represents $\hbar^2k_z^2/(2M)$, while the green dash-dotted curve represents Eq. (8) with $r_{\rm v} = 0.7095\xi$. The black solid curve represents the interpolating formula of Eq. (10). The inset shows the linear plot enlarged in the low-k_z region.

Here, we give a boundary condition similar to that of $f(r)$; $u'_{mlk_z}(R) = 0$, and $u_{mlk_z}(0) = 0$ [$u'_{mlk_z}(0) = 0$] when the centrifugal term in Eq. (6) exists for $l \neq -q$ [vanishes for $l = -q$], with similar notation for v_{mlk_z}.

The normal Kelvin wave corresponds to the core-localized mode with the angular quantum number $l = -1$ for a vortex with $q = 1$, whose dispersion relation and mode profile are shown in Fig. 1; these plots are obtained by numerically solving the BdG equation, and the numerical details are addressed in the next section. The Bogoliubov amplitude is

bounded at the vortex core, having a finite value at $r = 0$, as shown in Fig. 1(a). The excitation of this core-localized mode induces the finite amplitude at the vortex core, resulting in the displacement of the core position from $r = 0$. By taking into account the axial propagation $\propto e^{ik_z z}$ through Eqs. (2) and (3), the excitation actually involves helical deformation of the vortex core, as in the inset of Fig. 1(a). In Fig. 1(b), we show the log-log plot of the dispersion relation. When the condensate is confined in the finite-size container, the dispersion relation of the Kelvin wave has a small negative shift $\Delta = -\hbar^2/(MR^2)$ [55,56]; in Fig. 1(b), we thus subtract Δ from $\hbar\omega$, i.e., $\hbar\omega - \Delta \equiv \hbar\Omega$, to make a log-log plot. This negative shift is associated with the mode with a positive norm but negative energy for $k_z = 0$ [20,21]. The curve for $k_z \gg 1$ asymptotically approaches the single-particle behavior

$$\hbar\omega \simeq \frac{\hbar^2 k_z^2}{2M}. \tag{7}$$

In the low-k_z regime, the dispersion is given by the analytic expression derived in Ref. [56] as

$$\hbar\omega = \frac{\hbar^2 k_z^2}{2M}\left[\ln\frac{1}{k_z r_\mathrm{v}} - \chi(k_z R)\right]. \tag{8}$$

Here, r_v represents the cutoff length associated with the vortex-core structure, whose value is given analytically as

$$r_\mathrm{v} = \frac{e^{0.577-0.227}}{2}\xi \simeq 0.7095\xi. \tag{9}$$

In the following, we identify r_v as the vortex-core size. The function $\chi(k_z R)$ describes the correction of the finite-size effect, given as $\chi(x) = [K_0(x) + K_2(x)]/[I_0(x) + I_2(x)]$ with the modified Bessel functions I_n and K_n of the first and second kinds and the asymptotic behavior $\chi(x) \sim 2/x^2$ for $x \ll 1$ and $\chi(x) \sim \pi e^{-2x}$ for $x \gg 1$. Thus, the contribution $k_z^2\chi(k_z R)$ takes a value $2/R^2$ at $k_z = 0$ and converges rapidly to zero for $k_z\xi \gg \xi/R$ or $k_z R \gg 1$.

From the above-mentioned asymptotic behaviors, the Kelvin wave dispersion in the full range of k_z can be described by interpolating relations (7) and (8). Among the types of simple interpolating functions, we see in Appendix A that the arctangent-type function has the smallest difference from the numerical results. Thus, we suggest an interpolating formula of the Kelvin wave dispersion in the form

$$\hbar\omega_\mathrm{int} = \frac{\hbar^2 k_z^2}{2M}\left\{\ln\left[\frac{e}{\frac{2}{\pi}\arctan\left(\frac{\pi}{2}e r_\mathrm{v} k_z\right)}\right] - \chi(k_z R)\right\}. \tag{10}$$

For $r_\mathrm{v} k_z \ll 1$ the analytical formula in Eq. (8) is reproduced, while for $r_\mathrm{v} k_z \gg 1$ the quadratic relation $\hbar\omega_\mathrm{int} \sim \hbar^2 k_z^2/(2M)$ is obtained. Figure 1(b) shows that this interpolating formula reproduces the numerical result quite well. The difference between the numerical results and Eq. (10) is within 5% in the relevant range of k_z, as seen in Appendix A. We will apply this interpolating function, Eq. (10), to characterize the dispersion relation of the Kelvin wave in two-component BECs.

III. VORTEX-CORE SIZE IN TWO-COMPONENT BOSE-EINSTEIN CONDENSATES

Next, we seek the counterpart of the Kelvin wave of the axisymmetric vortex states in the miscible two-component BECs. Our focus is on clarifying the effects of the intercomponent interaction on the dispersion relation and the Bogoliubov amplitudes of the Kelvin mode. After introducing the formulation, we classify dynamically stable regimes of the vortex states in Sec. III A.

We expect that the dispersion relation of the Kelvin wave in two-component BECs can also be characterized by the vortex-core size. This hypothesis is based on the prospects: (i) The dispersion relation in a short-wavelength limit would also behave as a single-particle excitation. (ii) The dispersion relation in a long-wavelength limit would be influenced only by the cutoff length or the vortex-core size since microscopic features such as the internal structure of the vortex core would not have a direct impact on the large-scale collective dynamics. In the following, we will verify this expectation by evaluating the vortex-core size from the stationary solution in Sec. III B and extending the trial interpolating function (10) to the case of miscible binary condensates.

A. Dynamically stable vortices

The stationary state of the two-component BECs can be described by the coupled GP equations

$$\mu_j\Psi_j = \left(\hat{h}_j + \sum_{j'=1,2} g_{jj'}|\Psi_{j'}|^2\right)\Psi_j, \quad j = 1, 2. \tag{11}$$

Here, the single-particle Hamiltonian of the component j is $\hat{h}_j = -\hbar^2\nabla^2/(2M_j) + V_\mathrm{ext}^j(\boldsymbol{r})$, and the coupling constants are $g_{jj'}$. Like in Sec. II, the external potential $V_\mathrm{ext}^j(\boldsymbol{r})$ is taken to be zero and impose the Neumann boundary condition at $r = R$. In the homogeneous system, the mean-field theory predicts that two components experience phase separation when $g_{12}/\sqrt{g_{11}g_{22}} > 1$ is satisfied [57]. On the other hand, for $g_{12}/\sqrt{g_{11}g_{22}} < -1$, the condensates undergo a focusing collapse. In this work, we confine ourselves to the miscible regime $-1 < g_{12}/\sqrt{g_{11}g_{22}} < 1$, in which one can safely consider the dynamically stable vortex states. In the following, we fix the density in the bulk region as $|\Psi_1|^2 = |\Psi_2|^2 = n$ for simplicity and use the physical units determined by n. We here put $M_1 = M_2 = M$, $g_{11} = g_{22} = g$, and $\mu_1 = \mu_2 = gn(1 + \gamma)$, with the new parameter $g_{12}/g \equiv \gamma$. To this end, we present our results by using units independent of γ, namely,

$$\xi = \frac{\hbar}{\sqrt{Mgn}}, \quad \tau = \frac{\hbar}{gn} \tag{12}$$

for length and time, respectively, similar to those in Fig. 1 for a single-component BEC. These scales are useful to make clear the effect of intercomponent interaction γ on the properties of the Kelvin mode.

To consider a small fluctuation around the stationary solution, we write the wave function as $\Psi_j(\boldsymbol{r}, t) = \Psi_j(\boldsymbol{r}) + \delta\Psi_j(\boldsymbol{r}, t)$. Here, the stationary solutions can be written as

$$\Psi_j(r, \theta, z, t) = f_j(r)e^{iq_j\theta - i\mu_j t}, \tag{13}$$

with the real radial functions $f_1(r)$ and $f_2(r)$ and the vortex winding number q_1 and q_2. The fluctuation can be written as

$$\delta\Psi_j(\boldsymbol{r},t) = e^{iq_j\theta - i\mu_j t}\big[u_j(\boldsymbol{r},t) - v_j^*(\boldsymbol{r},t)\big]. \tag{14}$$

Along lines similar to the discussion in Sec. II, we consider the fluctuation by setting the ansatz as $u_j(\boldsymbol{r},t) = \sum_{m,l,k_z} u^{(j)}_{mlk_z}(r)e^{i(l\theta+k_z z-\omega t)}$ and $v_j(\boldsymbol{r},t) = \sum_{m,l,k_z} v^{(j)}_{mlk_z}(r)e^{i(l\theta+k_z z-\omega t)}$. The resulting BdG equation for the radial component reads

$$\mathcal{H}^{(lk_z)}\boldsymbol{w}_{mlk_z}(r) = \hbar\omega\boldsymbol{w}_{mlk_z}(r), \tag{15}$$

where

$$\boldsymbol{w}_{mlk_z}(r) = \big[u^{(1)}_{mlk_z}(r), v^{(1)}_{mlk_z}(r), u^{(2)}_{mlk_z}(r), v^{(2)}_{mlk_z}(r)\big]^{\mathrm{T}}, \tag{16}$$

$$\mathcal{H}^{(lk_z)} = \begin{pmatrix} \hat{h}^{+}_{lk_z,1} & -gf_1^2 & g_{12}f_1f_2 & -g_{12}f_1f_2 \\ gf_1^2 & -\hat{h}^{-}_{lk_z,1} & g_{12}f_1f_2 & -g_{12}f_1f_2 \\ g_{12}f_1f_2 & -g_{12}f_1f_2 & \hat{h}^{+}_{lk_z,2} & -gf_2^2 \\ g_{12}f_1f_2 & -g_{12}f_1f_2 & gf_2^2 & -\hat{h}^{-}_{lk_z,2} \end{pmatrix}, \tag{17}$$

$$h^{\pm}_{lk_z,j} = \frac{\hbar^2}{2M}\left(-\frac{\partial^2}{\partial r^2} - \frac{1}{r}\frac{\partial}{\partial r} + \frac{(q_j \pm l)^2}{r^2} + k_z^2\right) - \mu_j + 2gf_j^2 + g_{12}f_{j'}^2, \quad j' \neq j. \tag{18}$$

We solve this eigenvalue equation numerically to obtain the eigenvalue ω_{mlk_z} and the eigenfunctions $u^{(j)}_{mlk_z}(r)$ and $v^{(j)}_{mlk_z}(r)$ for given l and k_z.

For later discussion, it is useful to recall the excitation spectrum of the density oscillation for a homogeneous system without vortices ($q_1 = q_2 = 0$). In our simplified parameters, the excitation spectrum with respect to the wave number k in a homogeneous system is [58]

$$(\hbar\omega)^2_{\pm} = \frac{\hbar^2k^2}{2M}\left[\frac{\hbar^2k^2}{2M} + 2n(g \pm g_{12})\right]. \tag{19}$$

Here, we have two branches associated with the plus (minus) sign, corresponding to the in-phase (out-of-phase) oscillation of the two-component densities. In the low-k limit, we have the phonon dispersion $\omega \simeq \sqrt{gn(1\pm\gamma)/M}\,k$, while we have the single-particle spectrum $\omega \simeq \hbar^2k^2/(2M)$ in the high-k limit. For $\gamma > 0$, the out-of-phase branch approaches the quadratic relation $\omega_- \propto k^2$ as $\gamma \to 1$. Similarly, the in-phase branch becomes $\omega_+ \propto k^2$ as $\gamma \to -1$. These behaviors imply the instability associated with the phase separation at $\gamma = 1$ and focusing collapse at $\gamma = -1$.

Without loss of generality, we can consider the three cases of the axisymmetric vortex states with $(q_1, q_2) = (1, 1)$, $(1, 0)$, and $(1, -1)$. In the particular parameter regimes, these vortex states have dynamical instability associated with the appearance of the imaginary frequency of the Bogoliubov excitations, as summarized in Table I. Although we surmise this table from previous works [35,38,44], we give some supporting materials in Appendix B. We confine ourselves to considering Kelvin waves in the dynamically stable state. We expect that, even when there is small parameter asymmetry such as an imbalance of masses or of intracomponent scattering lengths, this stability diagram will not change. A systematic analysis including the full range of the parameter asymmetry would be an interesting perspective for future studies.

TABLE I. Diagram of the dynamical stability of axisymmetric vortex states in the two-component BECs based on past works through an analysis of the BdG equation (15) [35,38,44].

	$-1 < \gamma < 0$	$0 < \gamma < 1$
Case A, $q_1 = 1, q_2 = 1$	stable	unstable
Case B, $q_1 = 1, q_2 = 0$	stable	stable
Case C, $q_1 = 1, q_2 = -1$	unstable	unstable

B. Vortex-core size

In cases A and C in Table I, the axisymmetric vortex states consist of singly quantized vortices (SQVs) with vanishing total densities at $r = 0$, where both components have exactly the same density profile, $f_1(r)^2 = f_2(r)^2$. Then, the nonlinear term of the GP equation can be written as $g(1+\gamma)f_j(r)^3$. As a result, the vortex-core size is determined by the modified healing length $\xi/\sqrt{1+\gamma}$. To see this property, we numerically solve Eq. (11) and extract the vortex-core size by making the Gaussian fit $\propto e^{-r^2/(2\sigma^2)}$ to the profile $1 - f_j^2/n$. For $\gamma = 0$ we find that $\sigma \approx 1$, and the core size r_{v} can be reproduced when multiplying σ by a factor of 0.7095. According to this fitting analysis and $r_{\mathrm{v}} = 0.7095\sigma$, we determine the vortex-core size for $\gamma \neq 0$, as shown in Fig. 2(b). The core size for $\gamma > 0$ ($\gamma < 0$) decreases (increases) from that for $\gamma = 0$ and

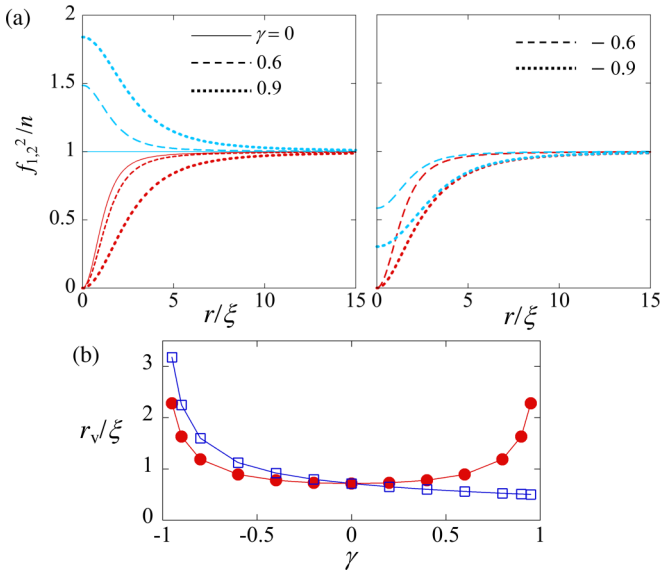

FIG. 2. (a) shows the radial density profile of the axisymmetric vortex state with $(q_1, q_2) = (1, 0)$ for several values of γ. The dark red and light blue curves represent $|\psi_1|^2$ and $|\psi_2|^2$, respectively, and the left and right panels correspond to the solutions for $\gamma \geqslant 0$ and $\gamma < 0$, respectively. (b) shows the vortex-core size, determined by the Gaussian fitting of the vortex-core profile, for $(q_1, q_2) = (1, 0)$ (solid circles) and $(q_1, q_2) = (1, 1)$ (open squares). The interpolating curves for the two plots are given by $r_{\mathrm{v}}/\xi = 0.7095/\sqrt{1-\gamma^2}$ and $r_{\mathrm{v}}/\xi = 0.7095/\sqrt{1+\gamma}$.

is written as

$$r_{\rm v} \simeq \frac{0.7095\xi}{\sqrt{1+\gamma}} \equiv r_{\rm SQV}. \tag{20}$$

In other words, the vortex solutions for different values of γ have profiles similar to Fig. 1(a) when we use the scaled coordinate $r\sqrt{1+\gamma}/\xi$.

For case B, we have a configuration of a half-quantized vortex (HQV) [33,36]. Figure 2(a) shows the stationary density profiles of the vortex states for $(q_1, q_2) = (1, 0)$ for several values of γ. For $\gamma > 0$ the intercomponent interaction is repulsive, so the vortex core is filled by the other nonrotating component to reduce the overlapping of the condensate density. For $\gamma < 0$, on the other hand, the density of the nonrotating component is reduced together with the density depletion of the vortex core. The size of the vortex core of the Ψ_1 component has a nontrivial dependence on γ, as shown in Fig. 2(b), where we show a Gaussian fitting analysis similar to case A for the density profile f_1^2. The core size behaves symmetrically with respect to the sign of γ. This is due to two length scales in our problem, namely, the "density" healing length $\xi_d = \xi/\sqrt{1+\gamma}$ and the "spin" healing length $\xi_s = \xi/\sqrt{1-\gamma}$ [33]. The former determines the spatial scale on which the total density $f_1^2 + f_2^2$ varies, and the latter does the same for the density difference $f_1^2 - f_2^2$. Since the asymptotic behaviors of the profile functions for $r \gg 1$ are written as $(f_1^2 + f_2^2)/n \sim 2 - \xi_d^2/r^2$ and $(f_1^2 - f_2^2)/n \sim -\xi_s^2/r^2$ [33], the profile for the first component is written as $f_1^2/n \sim 1 - (\xi_d^2 + \xi_s^2)/(2r^2)$. Thus, as shown in Fig. 2(b), the core size can be fitted as

$$r_{\rm v} = \frac{0.7095\xi}{\sqrt{1-\gamma^2}} \equiv r_{\rm HQV}. \tag{21}$$

IV. KELVIN WAVE IN TWO-COMPONENT BECs

In this section, we discuss the properties of the Kelvin wave for each vortex state by solving the BdG equation (15). From the above discussion, the structure of the vortex core is relevant for the properties of the Kelvin wave in two-component BECs through the ratio of the core size $r_{\rm v} = r_{\rm v}(\gamma)$ and the system size R as a finite-size effect. We thus fix the system size for a certain γ to $R/\xi = 30 r_{\rm v}(\gamma)/r_{\rm v}(0)$ throughout the following discussion to compare the results of the Kelvin wave for $\gamma = 0$.

A. Kelvin wave of a HQV

First, we consider the Kelvin wave for $(q_1, q_2) = (1, 0)$, i.e., a half-quantized vortex. As in the single-component BEC, the Kelvin mode corresponds to the lowest-energy mode with $l = -1$. The corresponding mode with $k_z = 0$ translates the vortex core without changing its internal structure. Then, the Bogoliubov amplitudes for finite k_z are also localized for both components, as shown in Fig. 3(a). For $\gamma > 0$ the amplitude $u^{(2)}_{mlk_z}$ of the nonvortex component takes the opposite sign of $u^{(1)}_{mlk_z}$ [the left panel of Fig. 3(a)]. This means that the density peak of Ψ_2 at the vortex core of Ψ_1 [see the left panel of Fig. 2(a)] decreases when the Kelvin wave is excited. Then, the denser region of the Ψ_2 component follows the displacement of the vortex core in Ψ_1. For $\gamma < 0$ the Bogoliubov amplitudes distribute similarly to the case of $\gamma > 0$, but the amplitude $u^{(2)}_{mlk_z}$ takes the same sign as $u^{(1)}_{mlk_z}$ [the right panel

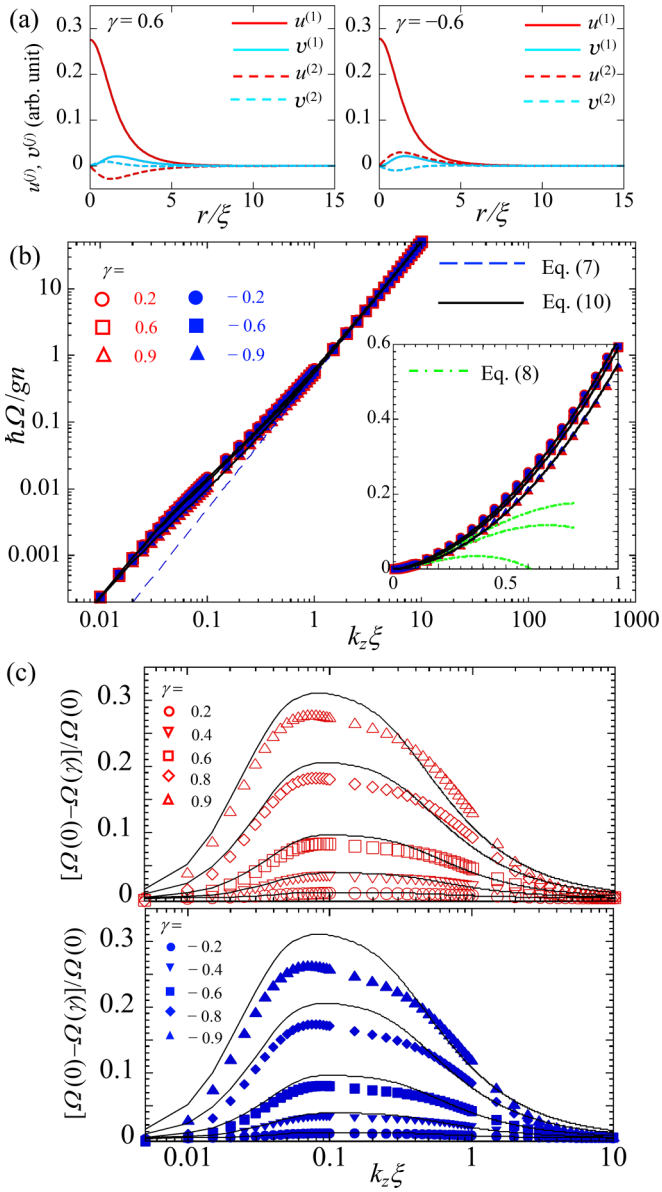

FIG. 3. The properties of the Kelvin wave $(l = -1)$ for $(q_1, q_2) = (1, 0)$. (a) The Bogoliubov amplitudes $u^{(1)}_{mlk_z}(r)$ (dark red solid curve), $v^1_{mlk_z}(r)$ (light blue solid curve), $u^{(2)}_{mlk_z}(r)$ (dark red dashed curve), and $v^2_{mlk_z}(r)$ (light blue dashed curve) with $(m, l, k_z) = (0, -1, \xi^{-1})$, which are typical for $\gamma > 0$ (left) and $\gamma < 0$ (right). (b) Log-log plots of the Kelvin wave dispersion are for several values of γ. The red open symbols for $\gamma > 0$ are almost coincident with the blue solid symbols for $\gamma < 0$ with the same magnitude $|\gamma|$. The solid, dashed, and dash-dotted curves refer to Eqs. (10), (7), and (8), respectively. The inset shows the linear plot enlarged in the low-k_z region, where the green dash-dotted curves are Eq. (8) with $r_{\rm v} = r_{\rm HQV}$ for $|\gamma| = 0.2$, 0.6, and 0.9 from top to bottom. In (c), we plot the difference of the dispersion relation from that for $\gamma = 0$. The solid curves represent the corresponding difference calculated from the interpolating formula (10) with $r_{\rm v} = r_{\rm HQV}$. The top and bottom panels show the results for $\gamma > 0$ and $\gamma < 0$, respectively.

of Fig. 3(a)]. This also implies that the density hollow of Ψ_2 [see the right panel of Fig. 2(a)] follows the displacement of the vortex core of Ψ_1 when the Kelvin wave is excited.

Figure 3(b) shows the dispersion relation of the Kelvin wave for $(q_1, q_2) = (1, 0)$ and various values of γ. To make a log-log plot, we subtract the negative-energy shift Δ at $k_z = 0$ as $\hbar\omega(\gamma) - \Delta(\gamma) = \hbar\Omega(\gamma)$ as in Fig. 1(b). All plots at $k_z\xi \gg 1$ asymptotically approach the quadratic function $\hbar^2 k_z^2/(2M)$, independent of the values of γ. This is because for $k_z\xi \gg 1$ the term $\hbar^2 k_z^2/(2M)$ in the diagonal component of Eq. (17) becomes dominant. However, the curvature of the dispersion curve in the low-k_z region has a weak dependence on γ, as seen in the inset of Fig. 3(b). We find that the analytic expression (8), in which $r_{\rm v}$ is replaced by $r_{\rm HQV}$ instead of 0.7095ξ, can describe well the dispersion in a low-k_z regime. To show this result more clearly, we plot in Fig. 3(c) the difference in the dispersion relation from that for $\gamma = 0$, i.e., that of the single-component BEC. Here, the difference is evaluated by $[\Omega(0) - \Omega(\gamma)]/\Omega(0)$. This γ dependence can be explained by the fact that the vortex-core size with $(q_1, q_2) = (1, 0)$ increases together with γ. To confirm this, we generate a similar plot, but now it is calculated from the interpolating formula in Eq. (10). Here, the core size $r_{\rm v}$ in Eq. (10) is also evaluated by $r_{\rm v} = r_{\rm HQV}$. The curves in Fig. 3(c) can capture the obtained γ dependence quite well.

We also note that the dispersion relations for $\gamma < 0$ are almost identical to those for $\gamma > 0$ with the same magnitude, as seen in Figs. 3(b) and 3(c). Thus, the dispersion relation behaves symmetrically with respect to the sign of γ, which supports the conclusion that the dispersion relation of the Kelvin wave is characterized by the vortex-core size of the vortical component, as expected from the γ^2 dependence of $r_{\rm v}$ in Fig. 2(b).

B. Kelvin wave of a SQV

Next, we consider the Kelvin wave for $(q_1, q_2) = (1, 1)$. In this setting, the vortex state is dynamically stable only for $\gamma \leqslant 0$. Since both components have a vortex, we can consider two branches of the Kelvin wave with nodeless radial modes, corresponding to the in-phase and out-of-phase oscillations (with a π-phase difference) of the helical vortex-line deformation. For $\gamma < 0$, the intercomponent attractive interaction energetically prefers the in-phase oscillation to the out-of-phase one, which is generally gapped since it involves the deformation of the vortex-core profile. We here discuss the two branches since both branches are gapless for $\gamma = 0$ and the out-of-phase Kelvin wave could have an excitation energy much lower than those of the other gapped modes when γ is sufficiently small.

Figure 4(a) shows a series of eigenvalues of the Bogoliubov modes with $l = -1$ for $\gamma = -0.6$ as a function of $k_z\xi$. The in-phase Kelvin mode corresponds to the lowest gapless mode, which is well separated from the other gapped excitation branches. This dispersion relation is well described by the interpolating formula of Eq. (10) with a suitable choice of $r_{\rm v}$ (see the following discussion). The out-of-phase Kelvin mode appears above a certain axial wave number $k_z\xi$ as a result of an avoided crossing of the two out-of-phase collective modes which are extended over the system in the low-k_z limit.

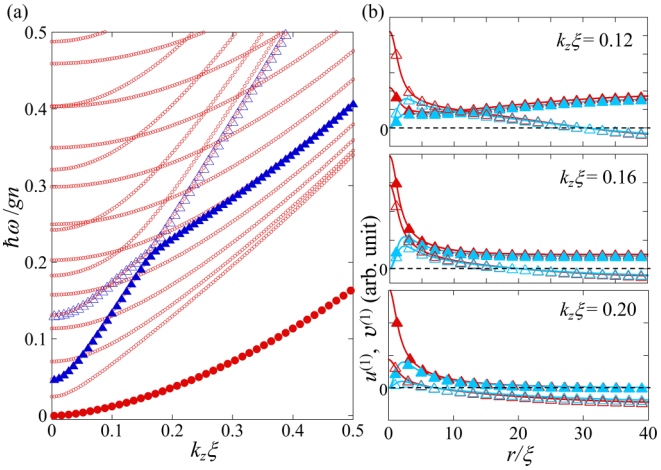

FIG. 4. (a) shows the dispersion relation of the Bogoliubov modes with $l = -1$ and various values of the radial quantum number m for $(q_1, q_2) = (1, 1)$ and $\gamma = -0.6$. The lowest mode (solid red circles) represents the in-phase Kelvin mode. The out-of-phase Kelvin mode emerges at $k_z\xi \gtrsim 0.16$ as a result of the avoided crossing of the two out-of-phase collective modes, shown by the blue solid and open triangles. In (b), we show the radial profile of the Bogoliubov modes $(u^{(1)}_{mlk_z}, v^{(1)}_{mlk_z})$ relevant to the avoided crossing in (a) for $k_z\xi = 0.12$, 0.16, and 0.2. The dark red curve and the light blue one with solid triangles correspond to the amplitudes $u^{(1)}_{mlk_z}$ and $v^{(1)}_{mlk_z}$, respectively, of the lower-lying mode [solid triangles in (a)], while those with open triangles correspond to the higher-lying mode [open triangles in (a)]. The profile of the second component is out-of-phase $(u^{(2)}_{mlk_z}, v^{(2)}_{mlk_z}) = -(u^{(1)}_{mlk_z}, v^{(1)}_{mlk_z})$, not shown here.

As shown in Fig. 4(a), the avoided crossing takes place at $k_z\xi = 0.16$, below which the two relevant modes are extended to the bulk region [top panel of Fig. 4(b)]. For $k_z\xi > 0.16$ the dispersion curve of the lower-lying mode approaches the quadratic form, and concurrently, its mode amplitudes are localized at the vortex core, as seen in the bottom panel of Fig. 4(b). Although we do not have a convincing explanation for why the out-of-phase mode arises from this avoided-crossing mechanism, the result means that it is difficult to separate overlapping vortex lines for a low-k_z regime without affecting the bulk region.

The dispersion relation of the in-phase mode for $\gamma < 0$ takes a form similar to that of the single-component BEC, being just Eq. (10) with $r_{\rm v} = r_{\rm SQV}$. This is because Eq. (15) with the conditions $f_1 = f_2$ and $(u^1_{mlk_z}, v^1_{mlk_z}) = (u^2_{mlk_z}, v^2_{mlk_z})$ owing to the in-phase mode reduces to the single-component BdG equation, so that one can reproduce the unique dispersion curve seen in Fig. 1 under a suitable scaling plot, apart from the finite-size correction $\chi(k_z R)$. Figure 5(a) shows the dispersion relations of the out-of-phase Kelvin mode for several values of γ, which also exhibit the quadratic dependence with respect to k_z at $k_z\xi \gg 1$. Thus, the out-of-phase mode in the high-k_z region can be written as $\hbar\omega \simeq \hbar^2 k_z^2/(2M) + \Delta\epsilon$ with a constant energy gap $\Delta\epsilon$. The energy gap arises from the fact that the relative displacement of the vortex cores in each component involves the deformation of the core structure and results in the energetic cost. In Fig. 5(b), we plot the energy gap $\Delta\epsilon$ as a function of γ. This γ dependence of $\Delta\epsilon$ can be

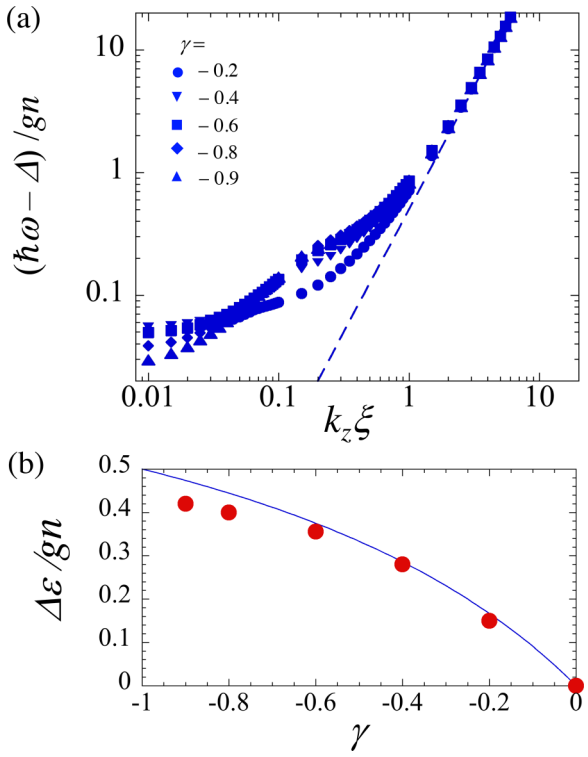

FIG. 5. In (a), log-log plots of the dispersion relations of the out-of-phase Kelvin mode are shown for several values of $\gamma(<0)$. The blue dashed line represents $\hbar^2 k_z^2/(2M)$. The curves in the lower-k_z region represent the frequency of the lower-lying out-of-phase mode contributing the avoided crossing. (b) shows the energy gap of the out-of-phase mode, extracted by the relation $\hbar\omega = \hbar^2 k_z^2/(2M) + \Delta\epsilon$ in the high-k_z region. The solid curve represents $\Delta\epsilon/(gn) = -\gamma/(1-\gamma)$.

fitted well by the relation $\Delta\epsilon \propto -\gamma/(1-\gamma)$, whose derivation needs more detailed consideration of the short-range properties of the vortex-vortex interaction.

V. CONCLUSION

In summary, we discussed the Kelvin wave of SQVs and HQVs in miscible two-component BECs. We first confirmed that the Kelvin wave dispersion of a single-component BEC is well described by the interpolating formula (10) in the whole range of k_z. Based on this interpolating formula and the precise evaluation of vortex-core properties, we considered the impact of the intercomponent interaction on the Kelvin mode by solving the BdG equation. For $(q_1, q_2) = (1, 0)$, the Kelvin wave dispersion is weakly dependent on the intercomponent interaction only through the change in the vortex-core size in the vortical component, which is written as Eq. (10) with $r_v = r_{HQV}$. Thus, the dispersion is symmetric with respect to the sign of the intercomponent coupling constant. In the case of $(q_1, q_2) = (1, 1)$ and the attractive intercomponent interaction $\gamma < 0$, we have both lower-lying in-phase and higher-lying out-of-phase branches for the Kelvin wave. The dispersion of the in-phase branch is gapless, written as Eq. (10) with $r_v = r_{SQV}$. The out-of-phase Kelvin wave is a gapped excitation, speculated to be generated from the avoided crossing of the two out-of-phase delocalized modes at low k_z. This energy gap is associated with the deformation of the vortex core caused by the relative displacement of the vortex position from the center.

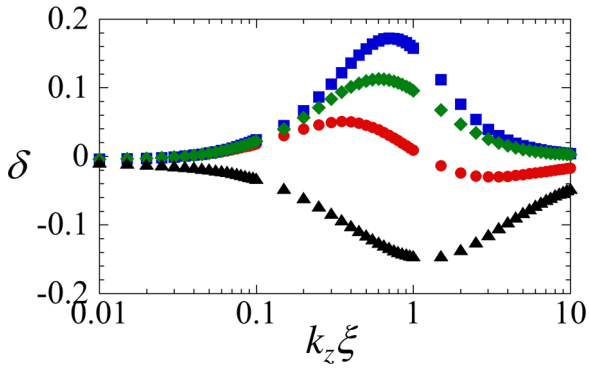

FIG. 6. The errors between the numerical data and Eq. (A1) with the interpolating function given by (A) $\arctan x$ (red circles), (B) $\tanh x$ (blue squares), (C) $x/\sqrt{1+x^2}$ (green diamonds), and (D) $x/(1+x)$ (black triangles). Here, the error is defined by $\delta \equiv (\Omega - \Omega_{int})/\Omega$.

ACKNOWLEDGMENTS

This research was supported by JSPS KAKENHI Grants No. JP18KK0391, No. JP20H01842, and No. 20H01843 and in part by the 2022 Osaka Metropolitan University (OMU) Strategic Research Promotion Project (Priority Research).

APPENDIX A: HOW TO DETERMINE AN INTERPOLATING FUNCTION BETWEEN EQS. (7) AND (8)

We here describe how to determine the interpolating functions in Eqs. (7) and (8) among several possible interpolating functions. To interpolate Eqs. (7) and (8), the logarithmic term of the dispersion relation of the Kelvin wave can be modified as

$$\hbar\omega_{int} = \frac{\hbar^2 k_z^2}{2M}\left[\ln\frac{e}{\phi(ek_z r_v)} - \chi(k_z R)\right]. \tag{A1}$$

Here, $\phi(x)$ $(x > 0)$ is an interpolating function satisfying the asymptotic behavior $\phi(x) \sim x$ for $x \ll 1$ and $\phi(x) \sim 1$ for $x \gg 1$. Note that the contribution $\chi(k_z R)$ from the finite-size effect converges to zero for $k_z R \gg 1$, so we do not need to consider it in the asymptotic limit at $x \gg 1$. We consider several simple functions satisfying the above asymptotic behavior: (A) $\phi(x) = (2/\pi)\arctan(\pi x/2)$, (B) $\phi(x) = \tanh(x)$, (C) $\phi(x) = x/\sqrt{1+x^2}$, and (D) $\phi(x) = x/(1+x)$. To seek the best choice that can reproduce the numerical results, we calculate the deviation of the interpolating function from the numerical one as $\delta = (\Omega - \Omega_{int})/\Omega$, where $\hbar\Omega = \hbar\omega - \Delta$ with the negative-energy shift Δ at $k_z = 0$ (see the main text). Among the above cases, choice A gives a better interpolation within 5% error in the intermediate range of $k_z\xi$, as shown in Fig. 6. We thus adopt Eq. (10) in the analysis.

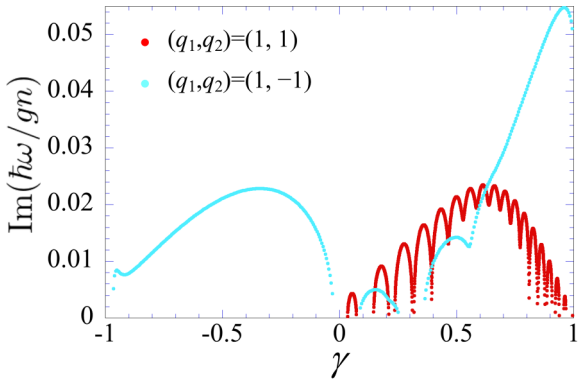

FIG. 7. The imaginary part of the eigenvalues of the BdG equation (15) for $l = 1$, $k_z = 0$, and $(q_1, q_2) = (1, 1)$ (dark red dots) and $(q_1, q_2) = (1, -1)$ (light blue dots) as a function of γ. The radius of the system is $R = 56\xi$.

APPENDIX B: THE BDG ANALYSIS SUPPORTING TABLE I

In this Appendix, we provide some discussion and numerical evidence which support the stability diagram in Table I. The dynamical stability of the vortex states can be studied through the analysis of the BdG equation (15) for $k_z = 0$. As shown in Fig. 7, the numerical solution reveals that an imaginary frequency appears in the range $0<\gamma<1$ for $(q_1, q_2) = (1, 1)$ (case A) and $-1<\gamma<1$ for $(q_1, q_2) = (1, -1)$ (case C), which is consistent with Table I.

For case A, the dynamically stable vortex configuration can take place only at $-1 < \gamma < 0$. This is because there is no relative velocity between the two components and the attractive intercomponent interaction energetically prefers the overlapping of vortex cores. Thus, the properties of the vortex state are similar to those of a single-component BEC. For $0 < \gamma < 1$ the overlapping vortices experience the splitting dynamical instability [38,44] induced by the repulsive intervortex interaction [36]. The bubble structure of the unstable domain shown in Fig. 7 is also seen in the splitting instability of a multiply quantized vortex in a single-component BEC [48–50,52,53].

For case C, we have a stationary vortex state similar to that in case A, but the counterrotating vortex state always gives rise to the dynamical instability for any value of γ [35,38]. In this regime, the local relative velocity between the two components increases near the vortex core and can locally exceed the critical velocity of the countersuperflow instability around the vortex-core region [35]. Thus, this instability also leads to the splitting of the overlapping vortex cores, which was demonstrated in Ref. [44] only for $0 < \gamma < 1$. In the case of $(q_1, q_2) = (1, 0)$ (case B), the local relative velocity also increases in the vortex core. However, the same argument does not necessarily hold since the density difference between the two components also increases. Since the HQV involves the smallest unit of circulation realized in this system, no further splitting can occur, and it is likely to be stable in the bulk.

[1] R. J. Donnelly, *Quantized Vortices in Helium II* (Cambridge University Press, Cambridge, 1991).
[2] A. L. Fetter, Rev. Mod. Phys. **81**, 647 (2009).
[3] K. G. Lagoudakis, M. Wouters, M. Richard, A. Baas, I. Carusotto, R. André, L. S. Dang, and B. Deveaud-Plédran, Nat. Phys. **4**, 706 (2008).
[4] L. Kelvin, Philos. Mag. **10**, 155 (1880).
[5] L. P. Pitaevskii, Sov. Phys. JETP **13**, 451 (1961).
[6] D. Kivotides, J. C. Vassilicos, D. C. Samuels, and C. F. Barenghi, Phys. Rev. Lett. **86**, 3080 (2001).
[7] W. F. Vinen, M. Tsubota, and A. Mitani, Phys. Rev. Lett. **91**, 135301 (2003).
[8] E. Kozik and B. Svistunov, Phys. Rev. Lett. **92**, 035301 (2004).
[9] V. S. L'vov, S. V. Nazarenko, and L. Skrbek, J. Low Temp. Phys. **145**, 125 (2006).
[10] V. S. L'vov and S. Nazarenko, JETP Lett. **91**, 428 (2010).
[11] A. W. Baggaley and C. F. Barenghi, Phys. Rev. B **83**, 134509 (2011).
[12] E. Sonin, Phys. Rev. B **85**, 104516 (2012).
[13] S. Autti, P. J. Heikkinen, S. M. Laine, J. T. Mäkinen, E. V. Thuneberg, V. V. Zavjalov, and V. B. Eltsov, Phys. Rev. Res. **3**, L032002 (2021).
[14] K. W. Madison, F. Chevy, W. Wohlleben, and J. Dalibard, Phys. Rev. Lett. **84**, 806 (2000).
[15] M. R. Matthews, B. P. Anderson, P. C. Haljan, D. S. Hall, C. E. Wieman, and E. A. Cornell, Phys. Rev. Lett. **83**, 2498 (1999).
[16] T. W. Neely, E. C. Samson, A. S. Bradley, M. J. Davis, and B. P. Anderson, Phys. Rev. Lett. **104**, 160401 (2010).
[17] V. Bretin, P. Rosenbusch, F. Chevy, G. V. Shlyapnikov, and J. Dalibard, Phys. Rev. Lett. **90**, 100403 (2003).
[18] S. Serafini, M. Barbiero, M. Debortoli, S. Donadello, F. Larcher, F. Dalfovo, G. Lamporesi, and G. Ferrari, Phys. Rev. Lett. **115**, 170402 (2015).
[19] S. Serafini, L. Galantucci, E. Iseni, T. Bienaimé, R. N. Bisset, C. F. Barenghi, F. Dalfovo, G. Lamporesi, and G. Ferrari, Phys. Rev. X **7**, 021031 (2017).
[20] A. L. Fetter and A. A. Svidzinsky, J. Phys.: Condens. Matter **13**, R135 (2001).
[21] A. L. Fetter, Phys. Rev. A **69**, 043617 (2004).
[22] T. P. Simula, T. Mizushima, and K. Machida, Phys. Rev. Lett. **101**, 020402 (2008).
[23] T. P. Simula, T. Mizushima, and K. Machida, Phys. Rev. A **78**, 053604 (2008).
[24] H. Takeuchi, K. Kasamatsu, and M. Tsubota, Phys. Rev. A **79**, 033619 (2009).
[25] T. P. Simula and K. Machida, Phys. Rev. A **82**, 063627 (2010).
[26] S. J. Rooney, P. B. Blakie, B. P. Anderson, and A. S. Bradley, Phys. Rev. A **84**, 023637 (2011).
[27] S. B. Papp, J. M. Pino, and C. E. Wieman, Phys. Rev. Lett. **101**, 040402 (2008).
[28] S. Tojo, Y. Taguchi, Y. Masuyama, T. Hayashi, H. Saito, and T. Hirano, Phys. Rev. A **82**, 033609 (2010).

[29] C. Cabrera, L. Tanzi, J. Sanz, B. Naylor, P. Thomas, P. Cheiney, and L. Tarruell, Science **359**, 301 (2018).
[30] G. Semeghini, G. Ferioli, L. Masi, C. Mazzinghi, L. Wolswijk, F. Minardi, M. Modugno, G. Modugno, M. Inguscio, and M. Fattori, Phys. Rev. Lett. **120**, 235301 (2018).
[31] D. V. Skryabin, Phys. Rev. A **63**, 013602 (2000).
[32] S. A. McGee and M. J. Holland, Phys. Rev. A **63**, 043608 (2001).
[33] M. Eto, K. Kasamatsu, M. Nitta, H. Takeuchi, and M. Tsubota, Phys. Rev. A **83**, 063603 (2011).
[34] T. Aioi, T. Kadokura, and H. Saito, Phys. Rev. A **85**, 023618 (2012).
[35] S. Ishino, M. Tsubota, and H. Takeuchi, Phys. Rev. A **88**, 063617 (2013).
[36] K. Kasamatsu, M. Eto, and M. Nitta, Phys. Rev. A **93**, 013615 (2016).
[37] L.-X. Wang, C.-Q. Dai, L. Wen, T. Liu, H.-F. Jiang, H. Saito, S.-G. Zhang, and X.-F. Zhang, Phys. Rev. A **97**, 063607 (2018).
[38] P. Kuopanportti, S. Bandyopadhyay, A. Roy, and D. Angom, Phys. Rev. A **100**, 033615 (2019).
[39] A. Richaud, V. Penna, and A. L. Fetter, Phys. Rev. A **103**, 023311 (2021).
[40] J. Han and M. Tsubota, Phys. Rev. A **103**, 053313 (2021).
[41] M. Edmonds, M. Eto, and M. Nitta, Phys. Rev. Res. **3**, 023085 (2021).
[42] V. P. Ruban, JETP Lett. **113**, 532 (2021).
[43] V. P. Ruban, J. Exp. Theor. Phys. **133**, 779 (2021).
[44] J. Han, K. Kasamatsu, and M. Tsubota, J. Phys. Soc. Jpn. **91**, 024401 (2022).
[45] S. Hayashi, M. Tsubota, and H. Takeuchi, Phys. Rev. A **87**, 063628 (2013).
[46] K. Kasamatsu, M. Tsubota, and M. Ueda, Int. J. Mod. Phys. B **19**, 1835 (2005).
[47] P. Kuopanportti, J. A. M. Huhtamäki, and M. Möttönen, Phys. Rev. A **85**, 043613 (2012).
[48] H. Pu, C. K. Law, J. H. Eberly, and N. P. Bigelow, Phys. Rev. A **59**, 1533 (1999).
[49] M. Möttönen, T. Mizushima, T. Isoshima, M. M. Salomaa, and K. Machida, Phys. Rev. A **68**, 023611 (2003).
[50] Y. Kawaguchi and T. Ohmi, Phys. Rev. A **70**, 043610 (2004).
[51] Y. Shin, M. Saba, M. Vengalattore, T. A. Pasquini, C. Sanner, A. E. Leanhardt, M. Prentiss, D. E. Pritchard, and W. Ketterle, Phys. Rev. Lett. **93**, 160406 (2004).
[52] E. Lundh and H. M. Nilsen, Phys. Rev. A **74**, 063620 (2006).
[53] H. Takeuchi, M. Kobayashi, and K. Kasamatsu, J. Phys. Soc. Jpn. **87**, 023601 (2018).
[54] We use a radial mesh size $\Delta r = 0.025\xi$, which is enough to yield accurate results that can reproduce the analytical evaluation in Ref. [56]. Also, we set the number of radial discretization points as $N_r = 1200$ based on our computational power. As a result, we choose $R = 30\xi$.
[55] M. Kobayashi and M. Nitta, Prog. Theor. Exp. Phys. **2014**, 21B01 (2014).
[56] D. A. Takahashi, M. Kobayashi, and M. Nitta, Phys. Rev. B **91**, 184501 (2015).
[57] P. Ao and S. T. Chui, Phys. Rev. A **58**, 4836 (1998).
[58] C. J. Pethick and H. Smith, *Bose–Einstein Condensation in Dilute Gases* (Cambridge University Press, Cambridge, 2008).